Density functional theory of soft matter

2002 J. Phys.: Condens. Matter 14 12147

(http://iopscience.iop.org/0953-8984/14/46/318)

INSTITUTE OF PHYSICS PUBLISHING JOURNAL OF PHYSICS: CONDENSED MATTER

J. Phys.: Condens. Matter **14** (2002) 12147–12158 PII: S0953-8984(02)38064-0

Density functional theory of soft matter

Hong Xu[1], **Laure Bellier-Castella**[1] **and Marc Baus**[2]

[1] Département de Physique des Matériaux (UMR 5586 du CNRS), Université Claude Bernard-Lyon1, 69622 Villeurbanne Cedex, France
[2] Physique des Polymères, Université Libre de Bruxelles, Campus Plaine, CP 223, B-1050 Brussels, Belgium

Received 12 June 2002, in final form 19 August 2002
Published 8 November 2002
Online at stacks.iop.org/JPhysCM/14/12147

Abstract

It is shown that the density functional theory (DFT) of soft matter is able to capture, in a semi-quantitative way, the essential properties of the phase behaviour in these complex systems. This is illustrated here for the case of the fractionation and segregation of polydisperse fluids of spherical (colloidal) particles and for the case of the self-assembling of monodisperse fluids of non-spherical particles. Both homogeneous and inhomogeneous situations will be considered and described within the same DFT.

1. Introduction

Since its first full-scale formulation in the seminal paper by Evans [1], the density functional theory (DFT) of inhomogeneous fluids has been applied with success to a great variety of physical situations. Most of the early applications of DFT to atomic fluids are well summarized in [2]. Its application to soft matter systems is less well developed, although the early results concerning, e.g., the freezing of hard sphere (HS) systems [3] and the superlattice formation of binary HS systems [4] are of direct relevance to the crystalline phases of specially prepared colloidal dispersions [5]. In the present paper we will review some ongoing work on the application of the DFT approach to soft matter systems with a special emphasis on

(1) the fractionation resulting from some underlying polydispersity [6–8],
(2) the segregation resulting from some spatial inhomogeneity [9, 10] and
(3) the self-assembling into anisotropic and non-uniform phases resulting from an anisotropic potential [11, 12].

The paper is organized as follows: in section 2, we consider the fluid–fluid and the fluid–solid fractionation of spherical polydisperse colloids. The segregation between the small and large colloidal spheres which occurs in a fluid–fluid interface or in a fluid under constant gravity will be studied in section 3. Section 4 is devoted to the study of the nematic and columnar phases of disc-shaped molecules. Our conclusions are gathered in the final section 5.

2. Fractionation in polydisperse bulk fluids

Polydispersity is a common feature of many colloidal dispersions [5]. In some cases it leads to intrinsically interesting phenomena, such as when studying the glass transition of HS colloids [13], or the phase behaviour of mixtures of hard rods and hard plates [14]. In many situations, however, it is a nuisance which obscures the phenomenon to be studied. Consequently, much effort has been devoted to limit its presence and nowadays well prepared colloidal dispersions are often considered to be monodisperse when compared to a theoretical model [15]. One reason for this is that, until quite recently, there were only very few studies of the phase behaviour of polydisperse systems. Although the basic equations were formulated some 20 years ago by Salacuse and Stell [16], only weakly polydisperse systems, whereby the width of the polydispersity distribution is treated as a smallness parameter, have been studied [17]. More recently, a new step was taken by Sollich *et al* [18] who introduced a 'projected free energy' whereby the original infinite-dimensional problem is transformed into a finite-dimensional one by annealing some of the moments of the polydispersity distribution. Although this simplifies the treatment of the polydispersity at a formal level, it has some drawbacks, the main one being that the coexistence (binodal) curves are inaccurate unless one includes some of the higher order moments, in which case one loses the main advantage of this method. Besides, it does not appear to be technically simpler than solving the equations resulting from the full (non-projected) free energy. Therefore, in what follows, we will simply use the full free-energy expression within a DFT framework for both the uniform and non-uniform systems to be considered. The variational principle of DFT and the phase equilibrium conditions lead then to exact equations which can be solved numerically to give either the coexistence curves to be considered here or the density profiles to be considered in the next section.

2.1. Fluid–fluid fractionation

To be specific, we consider an equilibrium system of spherical (colloidal) particles whose radii R_σ are distributed continuously within some interval, $R_{min} < R_\sigma < R_{max}$, centred on the reference value, R_0, usually taken to be the mean radius. When $R_{max} - R_{min} \to 0$, the system is said to be monodisperse whereas it is polydisperse whenever $R_{max} - R_{min} > 0$. The initial distribution of radii can then be characterized by its normalized probability distribution, $h_0(\sigma)$, where $\sigma = R_\sigma / R_0$ is the dimensionless polydispersity variable of 'species σ' of the continuous mixture. A specific situation will then usually be characterized by its polydispersity index I, or by $\sqrt{I-1}$. Here $I = m_2/(m_1)^2$, with m_n being the nth moment of the size distribution, so that $I = 1$ refers to a monodisperse situation. If the initial situation corresponds to a uniform fluid phase, the average number density of particles of species σ will be $\rho_0(\sigma) = \rho_0 h_0(\sigma)$, with ρ_0 the overall average number density. When the temperature is lowered it is often found that the initial fluid will phase separate into two fractions or daugther phases corresponding to $\rho_1(\sigma) = \rho_1 h_1(\sigma)$ and $\rho_2(\sigma) = \rho_2 h_2(\sigma)$. Such a fractionation combines thus some features of a fluid–fluid (say liquid–vapour) phase separation (e.g. $\rho_1 \neq \rho_2 \neq \rho_0$) with some features of a demixing transition (e.g. $h_1(\sigma) \neq h_2(\sigma) \neq h_0(\sigma)$). On further lowering of the temperature one may obtain more than two fractions [7] but for the sake of illustration we will limit our analysis here to two-phase fractionations only. The major difficulty of fractionation studies results from the coexistence of different size distributions. When the system is only weakly polydisperse ($I - 1 \ll 1$), simple fractionation rules can be found [19], but these have been shown [20] to be of limited value only. Some authors [21] have avoided the problem by imposing $h_1(\sigma) = h_2(\sigma) = h_0(\sigma)$, but this is generally untrue.

It is fairly straightforward [6] to study polydisperse fluids within the DFT formalism. To this end one can view the system as being inhomogeneous in species space and consider its density functional, $F[\rho]$, to be a functional of $\rho(\sigma)$. The chemical potential $\mu(\sigma,[\rho])$ of species σ can then be obtained as the functional derivative with respect to $\rho(\sigma)$ of the density functional per unit volume (V), $f[\rho] = F[\rho]/V$:

$$\mu(\sigma,[\rho]) = \delta f[\rho]/\delta\rho(\sigma); \tag{1}$$

whereas the pressure $p[\rho]$ can be obtained from

$$p[\rho] = \int \mathrm{d}\sigma\,\rho(\sigma)\mu(\sigma,[\rho]) - f[\rho]. \tag{2}$$

The equilibrium conditions for the two fractions, $\rho_1(\sigma)$ and $\rho_2(\sigma)$, namely, $\mu(\sigma,[\rho_1]) = \mu(\sigma,[\rho_2])$ and $p[\rho_1] = p[\rho_2]$, can be shown [6] to imply ($\beta = 1/k_BT$)

$$h_1(\sigma) = h_0(\sigma)\frac{\rho_2\exp(\beta\{\mu_{ex}(\sigma;[\rho_2]) - \mu_{ex}(\sigma;[\rho_1])\})}{x_2\rho_1 + x_1\rho_2\exp(\beta\{\mu_{ex}(\sigma;[\rho_2]) - \mu_{ex}(\sigma;[\rho_1])\})} \tag{3}$$

where $x_1(x_2)$ is the fraction of particles in phase 1 (or 2). They are related to the densities by the Lever rule: $x_1 = \frac{\rho_1}{\rho_1-\rho_2}\frac{\rho_0-\rho_2}{\rho_0}$ and $x_2 = 1 - x_1$. Having obtained $h_1(\sigma)$ from equation (3), the particle number conservation gives

$$h_2(\sigma) = \frac{\rho_0(\rho_2-\rho_1)}{\rho_2(\rho_0-\rho_1)}h_0(\sigma) + \frac{\rho_1(\rho_0-\rho_2)}{\rho_2(\rho_0-\rho_1)}h_1(\sigma) \tag{4}$$

where $\mu_{ex}(\sigma,[\rho])$ is the excess part of $\mu(\sigma,[\rho])$. To solve equations (1)–(3) we need to know the explicit expression of $h_0(\sigma)$ and $f[\rho]$. For $h_0(\sigma)$ we have taken here the widely used Schulz–Zimm distribution, which will be used throughout:

$$h_0(\sigma) = \alpha^\alpha(1+\sigma)^{\alpha-1}\mathrm{e}^{-\alpha(1+\sigma)}/\,\Gamma(\alpha) \tag{5}$$

where $I = 1 + \frac{1}{\alpha}$ and $\Gamma(\alpha)$ is the Euler gamma-function. For illustrative purposes we took $f[\rho]$ to be of the following van der Waals (vdW) form:

$$f[\rho] = k_BT\int \mathrm{d}\sigma\,\rho(\sigma)\left\{\ln\left(\frac{\Lambda^3(\sigma)\rho(\sigma)}{E[\rho]}\right) - 1\right\} + \frac{1}{2}\int\mathrm{d}\sigma\int\mathrm{d}\sigma'\,V(\sigma,\sigma')\rho(\sigma)\rho(\sigma') \tag{6}$$

where $\Lambda(\sigma)$ is the thermal de Broglie wavelength resulting from the kinetic energy, $E[\rho]$ the vdW excluded volume resulting from the repulsions

$$E[\rho] = 1 - \frac{1}{\eta_m}\int\mathrm{d}\sigma\,v(\sigma)\rho(\sigma) \tag{7}$$

where $v(\sigma) = \sigma^3 v_0$, $\eta_m = \rho_m v_0$ with $v_0 = \frac{4\pi}{3}(R_0)^3$ being the volume of the reference particle of radius R_0 and ρ_m is the maximum density of the fluid phase. Finally, in equation (6), $V(\sigma,\sigma')$ represents the cohesion energy density resulting from the attractions. Since there is at present no experimental information on how $V(\sigma,\sigma')$ depends on the polydispersity variables we have taken it to be of the simple form $V(\sigma,\sigma') = -\epsilon_0\sigma\sigma' v_0(\sigma+\sigma')^3$, where ϵ_0 sets the energy scale. Polydispersity favours phase separation, by enlarging the two-phase region, and modifies many of its features [6]. Here we will focus our attention on the fractionation properties. An example of a solution of equations (3), (4) for h_0 given by equation (5) with $\alpha = 55$ or $I = 1.018$, $\rho_0 v_0 = 0.33$, $\eta_m = 1$ and $f[\rho]$ by equations (6)–(7) with $k_BT/\epsilon_0 = 1$ is given in figure 1. It is seen that one of the fractions (the low density or 'vapour' phase 1, $\rho_1 v_0 = 0.11$) is enriched in small ($\sigma < 1$) particles ($m_1(1) = 0.93 < 1$) whereas the other fraction (the high density or 'liquid' phase 2, $\rho_2 v_0 = 0.60$) is enriched with large ($\sigma > 1$) particles ($m_1(2) = 1.02 > 1$) relative to the original (parent) phase ($\rho_0 v_0 = 0.33$, $m_1(0) = 1$). Here, $m_n(p)$ denotes the nth moment of the distribution $h_p(\sigma)$ of the phase p. Note also

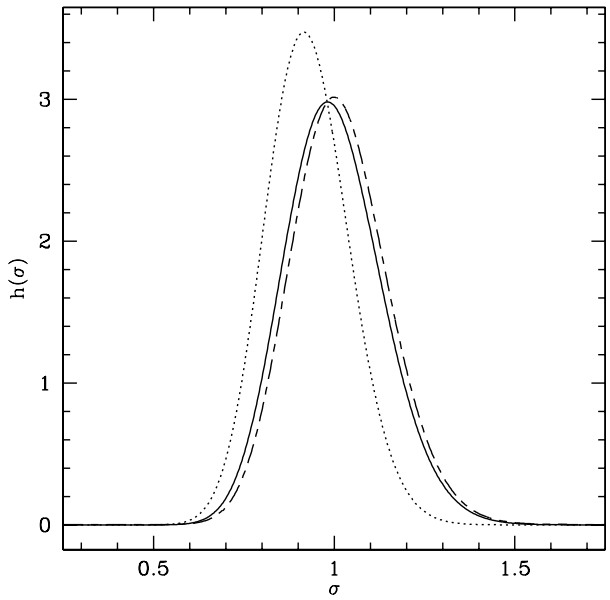

Figure 1. Fractionation of an initial polydisperse fluid phase (full curve) of density $\eta = 0.33$, temperature $k_B T/\epsilon_0 = 1$ and a (Schulz–Zimm) size distribution of polydispersity index $I = 1.018$ into a low density fraction (dotted curve) enriched in small particles and a high density fraction (dot–dashed curve) enriched in large particles. Shown are the normalized size distributions $h(\sigma)$ versus the reduced particle radius σ.

that the distributions of the two fractions have a smaller variance ($m_2(1) - m_1^2(1) = 0.0051$, $m_2(2) - m_1^2(2) = 0.0096$) than the parent phase ($m_2(0) - m_1^2(0) = 0.02$) leading to a reduced overall polydispersity ($I(1) = 1.016$, $I(2) = 1.017$) of the fractions. Repeated fractionation is indeed a standard experimental technique to produce less poydisperse samples.

2.2. Fluid–solid fractionation

The phenomenon of bulk phase fractionation is however not limited to fluid phases only. Upon freezing a bulk fluid will generally fractionate into two bulk fractions with different structures, different densities and different size distributions. Because of the numerical difficulty of a simultaneous treatment of the spatial and species non-uniformities this problem has however not yet been addressed theoretically. Indeed, in their seminal work on polydisperse HS colloids, Barrat and Hansen [22] only performed a stability analysis for a specific crystal structure and found that the crystal phase becomes unstable above a limiting polydispersity threshold. This result was confirmed later by simulations [23], while in a more recent theoretical investigation [21] fractionation was neglected (e.g. by imposing $h_1(\sigma) = h_2(\sigma) = h_0(\sigma)$) altogether. The unavoidable presence of fractionation in polydisperse systems can however be illustrated here by adapting the above DFT to HS systems. To this end we put $V(\sigma, \sigma') = 0$ in equation (6) and describe hence the HS fluid (phase 1) by

$$f_1[\rho] = k_B T \int \mathrm{d}\sigma\, \rho(\sigma) \left\{ \ln\left(\frac{\Lambda^3(\sigma)\rho(\sigma)}{E_1[\rho]} \right) - 1 \right\} \tag{8}$$

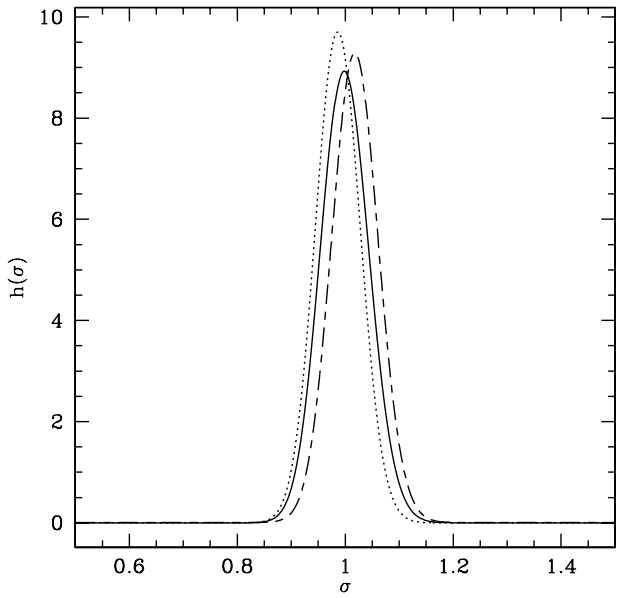

Figure 2. Fractionation of a polydisperse HS fluid (full curve) of density $\eta_0 = 0.53$, polydispersity index $I = 1.002$ into a fluid (dotted curve) and a solid (dot–dashed curve) fraction enriched, respectively, with small and large particles (see also figure 1).

with $E_1[\rho]$ given by equation (7). Within the same vdW excluded volume approach, the HS solid (phase 2) can then be similarly described by

$$f_2[\rho] = k_B T \int \mathrm{d}\sigma\, \rho(\sigma) \left\{ \ln\left(\frac{\Lambda^3(\sigma)\rho(\sigma)}{E_2[\rho]} \right) - 1 \right\} \tag{9}$$

where $E_2[\rho]$ can be obtained from a free-volume theory as [24]

$$E_2[\rho] = \left\{ 1 - \left(\frac{1}{\eta_{cp}} \int \mathrm{d}\sigma\, v(\sigma)\rho(\sigma) \right)^{1/3} \right\}^3 \tag{10}$$

with $\eta_{cp} = \rho_{cp} v_0$ the maximum packing fraction of the solid phase. Equation (9) will provide, of course, only a crude approximation of the solid since it sidesteps the intrinsic lattice-periodic non-uniformity of the density in a solid, the latter being described here only in terms of its spatially averaged density $\rho(\sigma)$. Nevertheless, the difference in functional form of the excluded volume in the fluid and solid phases (compare $E_1[\rho]$ and $E_2[\rho]$), and therefore in the underlying equations of state, is sufficient to adequately locate the HS fluid–solid transition in the monodisperse HS system [24]. Note, however, that while when only fluid phases are considered the parameter η_m which appears in equation (7) is immaterial, since it only sets the density scale; this is no longer the case when the fluid competes with the solid. In such a situation it was found [24] that taking, e.g., $\eta_m = 1/8 + \eta_{cp}/2$ leads to a reasonable HS fluid–solid transition in the monodisperse case. We will hence adopt the same value for η_m here. Finally, the value of η_{cp} could be influenced by the polydispersity of the solid but to avoid too great a complexity we will adopt here the value $\eta_{cp} = \pi/3\sqrt{2}$, corresponding to a monodisperse close-packed lattice structure. Under these conditions a polydisperse HS fluid of initial density $\eta_0 = 0.53$ and small initial polydispersity $I = 1.002$ (namely $\alpha = 500$ in equation (5)) will fractionate into a polydisperse fluid and solid as shown in figure 2. The fluid (phase 1) has a lower density ($\eta_1 = 0.49$), is enriched in small particles ($m_1(1) = 0.987$) and

has a smaller variance ($m_2(1)-m_1^2(1) = 8.3\times10^{-4}$) and a smaller polydispersity ($I_1 = 1.0017$) than the parent phase, whereas the solid (phase 2) has a higher density ($\eta_2 = 0.59$), is enriched in large particles ($m_1(2) = 1.0178$) and has a smaller variance ($m_2(2) - m_1^2(2) = 1.98\times10^{-3}$) and a smaller polydispersity ($I_2 = 1.0018$) than the initial phase. When the polydispersity is increased, the illustrated accumulation of the larger particles into the solid phase will ultimately destabilize the latter. Note however that the solid phase may prevent this by fractionating into two solid phases of lower polydispersity.

3. Segregation in inhomogeneous polydisperse fluids

In section 2 we only considered situations where the density depends on only one variable, namely $\rho(\sigma)$. As soon as we take into account the presence of an external field such as gravity, the latter will break the translational invariance of the system and its density will become space dependent, namely $\rho(\boldsymbol{r},\sigma)$. If $\Phi(\boldsymbol{r},\sigma)$ represents the potential from which the external field derives, then the chemical potential $\mu(\sigma,[\rho])$ of the inhomogeneous system of density $\rho(\boldsymbol{r},\sigma)$ will be given by

$$\mu(\sigma) = \Phi(\boldsymbol{r},\sigma) + \left.\frac{\delta F[\rho]}{\delta\rho(\boldsymbol{r},\sigma)}\right|_T. \tag{11}$$

This Euler–Lagrange equation expresses the constancy of the chemical potential throughout the inhomogeneous equilibrium system. To solve equation (11) for the four-variable function $\rho(\boldsymbol{r},\sigma)$ constitutes, even for the simple density functionals $F[\rho]$ considered in section 2, a formidable numerical problem. Nevertheless, when the external field has a fixed direction and the translational invariance is broken only along the z-axis so that the density will depend only on two variables, namely $\rho(z,\sigma)$, one can solve equation (11) for a few simple situations as we now show.

3.1. Polydisperse fluid with a planar interface

Consider again the polydisperse vdW fluid studied in section 2.1 and assume that T is such that the system fractionates into two fluid fractions. The external gravity field will spatially separate the two fractions according to their density and the system will build up an interface sandwiched between two bulk phases. Under such circumstances the influence of the external field can be replaced by an appropriate boundary condition. For sufficiently weak fields we can indeed now solve equation (11) without the external field and look for a solution, say $\rho(z,\sigma)$, which asymptotically (i.e. when $z\to\pm\infty$) matches the densities (say $\rho_\pm(\sigma)$) of the two coexisting bulk phases. Moreover, since the chemical potential of the two bulk phases is known (cf section 2.1) and the chemical potential of the system has to remain constant, we can eliminate the latter from equation (11) and, as shown elsewhere [9], end up with two equivalent integral equations of the form

$$\rho(z,\sigma) = A_0^{\pm}(z)M^{\pm}(z,\sigma) \tag{12}$$

where $A_0^{\pm}(z)$:

$$A_0^{\pm}(z) = \frac{1-\eta_0(z)}{1-\eta_0^{\pm}}\exp\left\{\frac{1}{1-\eta_0^{\pm}} - \frac{1}{1-\eta_0(z)}\right\} \tag{13}$$

involves only the zeroth-order σ-moment of $\rho(z,\sigma)$, namely $\eta_0(z) = v_0\int \mathrm{d}\sigma\,\rho(z,\sigma)$ and $\eta_0^{\pm} = \eta_0(z=\pm\infty)$, whereas $M^{\pm}(z,\sigma)$ reads

$$M^{\pm}(z,\sigma) = \rho_{\pm}(\sigma)\exp\left[\sigma\int_{-\infty}^{\infty}\mathrm{d}z'\,\beta\,V_1(|z-z'|)\{\eta_1^{\pm}-\eta_1(z')\}\right] \tag{14}$$

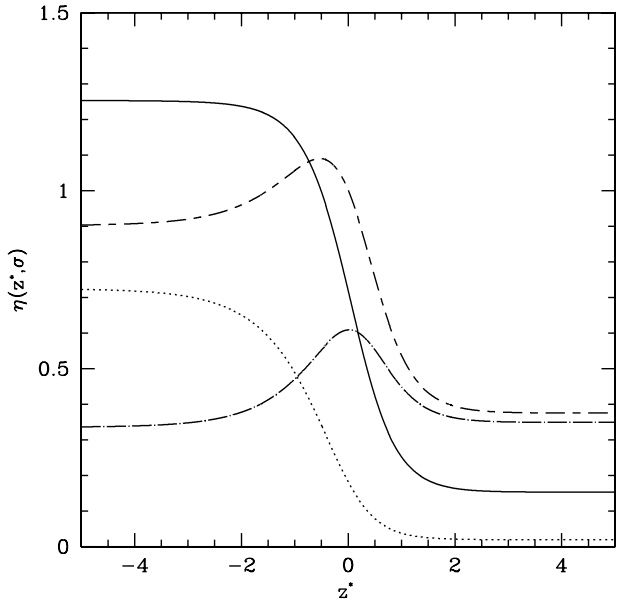

Figure 3. Reduced density profiles, $\eta(z^*, \sigma) = v_0\rho(z^*, \sigma)$, versus the reduced distance to the interface, $z^* = z/R_0$, of a planar fluid–fluid interface for $\sigma = 1.25$ (dotted curve), 1 (solid curve), 0.8 (dash–dash curve) and 0.65 (dot–dash curve). The initial density and polydispersity index correspond to $\eta_0 = 0.484$ and $I = 1.067$, respectively, while the temperature is $k_BT/\epsilon_0 = 0.85$. Note the segregation of the small ($\sigma < 1$) particles towards the interface.

where $\eta_1(z) = v_0 \int \mathrm{d}\sigma\, \sigma\rho(z, \sigma)$, $\eta_1^{\pm} = \eta_1(z = \pm\infty)$, $\rho_{\pm}(\sigma) = \rho(z = \pm\infty, \sigma)$ and $V_1(|z|)$ is the lateral interaction potential [9] (namely, $V_1(z) \propto \int \mathrm{d}x \int \mathrm{d}y\, V(r)$), which for simplicity we took to be Gaussian. Note that in the above, we also simplified the dependence of $F[\rho]$ on the polydispersity by putting $v(\sigma) = v_0$ and $V(\sigma, \sigma') = \sigma\sigma' V(1, 1)$ in the vdW model of section 2.1, since this does not alter qualitatively the phase coexistence results while simplifying the numerical treatment [6]. In figure 3 we show some results for the $\rho(z, \sigma)$ obtained in this way. It is seen that while the large ($\sigma > 1$) particles have a density profiles which smoothly interpolates between the two bulk values ($\rho_-(\sigma)$ and $\rho_+(\sigma)$) the small ($\sigma < 1$) particles segregate out of the two bulk phases and accumulate in the interfacial region.

3.2. Sedimentation profiles

We now consider a polydisperse fluid in a confined geometry ($0 < z < \infty$) under the influence of an external gravity field corresponding to $\Phi(z, \sigma) = m(\sigma)gz$, where $m(\sigma)$ is the mass of species σ and g is the gravity constant. Here the resulting sedimentation profile will thus again depend only on two variables, namely $\rho(z, \sigma)$. The boundary condition is now $\rho_+(\sigma) \equiv \rho(z = +\infty, \sigma) = 0$, whereas the particle number conservation implies for each σ

$$\lim_{L\to\infty} \frac{1}{L} \int_0^L \mathrm{d}z\, \rho(z, \sigma) = \rho_0(\sigma) \tag{15}$$

where $\rho_0(\sigma)$ is the initial size distribution, assumed to be known (cf equation (5)). Equation (11) implies now

$$\rho(z, \sigma) = \left(\frac{(1 - \eta_0(z))}{\Lambda^3(\sigma)}\right) \exp\left[\beta\mu(\sigma) - \beta\Phi(z, \sigma) - \frac{\eta_0(z)}{1 - \eta_0(z)} - 8\beta\epsilon_0\sigma\eta_1(z)\right] \tag{16}$$

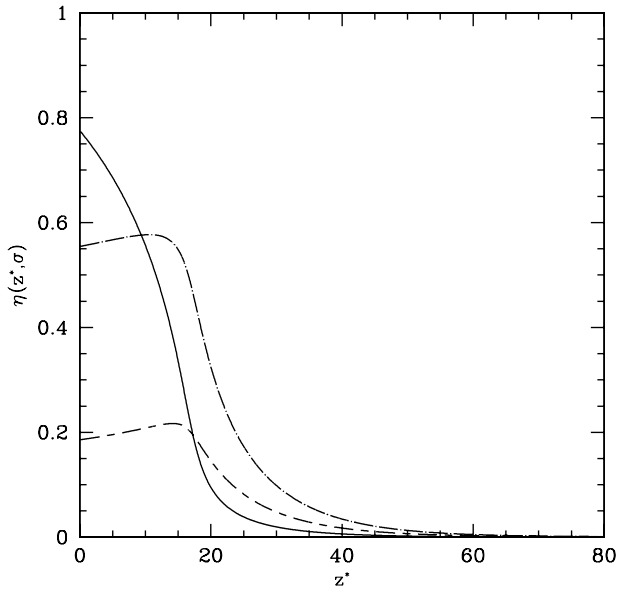

Figure 4. Reduced density profiles, $\eta(z^*, \sigma) = v_0\rho(z^*, \sigma)$, versus the reduced distance, $z^* = z/R_0$, of a polydisperse fluid confined to the $z^* \geqslant 0$ half-space under the influence of a constant gravity field for $\sigma = 1.25$ (full curve), 0.75 (dot–dash curve) and 0.65 (dash–dash curve). The initial density and polydispersity index correspond to $\rho_0 v_0 = 0.087$ and $I = 1.04$, respectively, while the temperature is $k_BT/\epsilon_0 = 1.5$ and $m_0 g R_0/k_BT = 0.1$. Note the segregation of the small ($\sigma < 1$) particles towards the intermediate heights.

where $\eta_n(z) = v_0 \int \mathrm{d}\sigma\, \sigma^n \rho(z, \sigma)$ with $n = 0$, 1, and ϵ_0 sets the energy scale of the attractions. To obtain equation (16) we have again simplified the polydispersity dependence of the vdW model of section 2.1 by taking $v(\sigma) = v_0$ (hence $m(\sigma) = m_0$) and $V(\sigma, \sigma') = \sigma\sigma' V(1, 1)$. We have moreover localized the density functional $F[\rho]$ by taking the lateral interaction $V_1(|z|)$ to be a Gaussian of zero width. Such a local density approximation is known to be reasonable provided $mgR_0 \ll k_BT$, i.e. T large enough [26]. Substitution of the $\rho(z, \sigma)$ of equation (16) into (15) fixes in principle $\mu(\sigma)$ but in order to keep the problem tractable, we have approximated $\mu(\sigma)$ by

$$\beta\mu(\sigma) = \ln(\Lambda^3(\sigma)\rho_0(\sigma)) + \sum_{i=0}^{n} a_i(\sigma - 1)^i \tag{17}$$

and determined the n coefficients a_i (in practice we took $n = 3$) by minimizing $|\lim_{L\to\infty}(1/L)\int_0^L \mathrm{d}z\, \rho(z, \sigma) - \rho_0(\sigma)|$ (cf equation (15)). Solving equations (15)–(17) iteratively [10] one obtains the profiles shown in figure 4 (with equation (15) being satisfied within 10^{-4}). It is seen that while the large ($\sigma > 1$) particles have a monotonically decreasing density profile, as expected for a sedimentation experiment, the small ($\sigma < 1$) particles have a non-monotonic profile exhibiting a maximum in the region where the density profile of the large particles exhibits its largest gradient. In other words, the small particles are partially expelled from the bottom of the vessel by the large particles, a non-monotonic feature which results from the delicate balance between the excluded volume effects and those due to the attractions and the external field. We notice that local size segregation has also been predicted for polydisperse HS fluids near a wall [27].

4. Self-assembling into liquid-crystalline phases of monodisperse discotic molecules

Whereas in the previous sections 2 and 3 we used DFT methods to study (colloidal) systems composed of spherical particles with a size polydispersity, in the present section we will consider the application of DFT methods to the study of monodisperse (molecular) systems of non-spherical particles. At the formal level, there exists a close relationship between these two types of system because in both cases the one-particle density depends on, besides the position $\boldsymbol{r}$ of the particle, one extra variable. For the colloidal systems considered above this was the polydispersity variable σ related to the size of the spherical particles (cf $\rho(\boldsymbol{r}, \sigma)$) whereas here it is the orientation of the non-spherical particles, say $\rho(\boldsymbol{r}, \boldsymbol{u})$, if $\boldsymbol{u}$ denotes a unit vector along, say, the symmetry axis of a uniaxial centro-symmetric molecule. Indeed, as is well known since Onsager's work [28], a monodisperse system of non-spherical particles can also be viewed as a system of 'spherical' particles with a polydispersity in their orientations ($\boldsymbol{u}$). This analogy is however not complete because here $\boldsymbol{u}$ is a vector while σ is a scalar and, more fundamentally, the size distribution $\rho(\sigma)$ is monitored by the initial parent-phase size distribution ($\rho_0(\sigma)$) whereas here the angular distribution $\rho(\boldsymbol{u})$ has to minimize the free-energy functional (usually within a given class of trial functions, as done below). Nevertheless, this analogy is very useful because it allows one to transpose easily theoretical treatments from one system to another, as we now illustrate (see also [11]).

4.1. The density functional

For a system of identical uni-axial centro-symmetric molecules whose number density is $\rho(\boldsymbol{r}, \boldsymbol{u})$, with $\boldsymbol{r}$ denoting the position of the centre of symmetry and $\boldsymbol{u}$ being a unit vector ($\boldsymbol{u}^2 = 1$) along the symmetry axis, the free-energy density functional per unit volume, $f[\rho]$, can be split into an ideal and an excess part, with the former given by

$$f_{id}[\rho] = k_B T \int \frac{\mathrm{d}\boldsymbol{x}}{V} \rho(\boldsymbol{x}) \{\ln(\Lambda^3 \rho(\boldsymbol{x})) - 1\} \tag{18}$$

where $\boldsymbol{x} = \{\boldsymbol{r}, \boldsymbol{u}\}$ and $\mathrm{d}\boldsymbol{x} = \mathrm{d}\boldsymbol{u}\,\mathrm{d}\boldsymbol{r}$, with $\int \mathrm{d}\boldsymbol{r} = V$, and $\int \mathrm{d}\boldsymbol{u} = 1$, or in spherical coordinates, $\boldsymbol{u}(\theta, \phi)$, $\mathrm{d}\boldsymbol{u} = \frac{1}{4\pi}\,\mathrm{d}\phi\,\mathrm{d}\theta\sin\theta$. If the molecules interact via a pair-potential, $V(\boldsymbol{x}_1, \boldsymbol{x}_2)$, we can approximate the excess term, $f_{ex}[\rho]$, by first splitting this potential into an attractive (A) and a repulsive (R) contribution, $V(\boldsymbol{x}_1, \boldsymbol{x}_2) = V_A(\boldsymbol{x}_1, \boldsymbol{x}_2) + V_R(\boldsymbol{x}_1, \boldsymbol{x}_2)$, and evaluating the contribution of $V_A(\boldsymbol{x}_1, \boldsymbol{x}_2)$ to $f_{ex}[\rho]$ in a vdW mean-field manner:

$$f_{ex}^A[\rho] = \frac{1}{2V} \int \mathrm{d}\boldsymbol{x}_1 \int \mathrm{d}\boldsymbol{x}_2\, \rho(\boldsymbol{x}_1)\rho(\boldsymbol{x}_2) V_A(\boldsymbol{x}_1, \boldsymbol{x}_2) \mathrm{e}^{-\beta V_R(\boldsymbol{x}_1, \boldsymbol{x}_2)} \tag{19}$$

and the contribution of $V_R(\boldsymbol{x}_1, \boldsymbol{x}_2)$ to $f_{ex}[\rho]$ in the following generalized Onsager fashion:

$$f_{ex}^R[\rho] = \frac{k_B T}{V} \int \mathrm{d}\boldsymbol{r}\, \rho(\boldsymbol{r}) \Psi(v_0 \bar{\rho}(\boldsymbol{r})) \tag{20}$$

adapted from [29]. Note that in equation (20), $\rho(\boldsymbol{r})$ and $\bar{\rho}(\boldsymbol{r})$ denote, respectively, the orientationally averaged density, $\rho(\boldsymbol{r}) = \int \mathrm{d}\boldsymbol{u}\, \rho(\boldsymbol{r}, \boldsymbol{u})$, and the effective density

$$\bar{\rho}(\boldsymbol{r}) = \frac{1}{2B_2 \rho(\boldsymbol{r})} \int \mathrm{d}\boldsymbol{x}_1\, \delta(\boldsymbol{r} - \boldsymbol{r}_1) \int \mathrm{d}\boldsymbol{x}_2\, \rho(\boldsymbol{x}_1)\rho(\boldsymbol{x}_2)(1 - \mathrm{e}^{-\beta V_R(\boldsymbol{x}_1, \boldsymbol{x}_2)}) \tag{21}$$

the latter being constructed in such a manner that at low density equation (20) will yield the exact second virial coefficient B_2:

$$B_2 = \frac{1}{2V} \int \mathrm{d}\boldsymbol{x}_1 \int \mathrm{d}\boldsymbol{x}_2\, (1 - \mathrm{e}^{-\beta V_R(\boldsymbol{x}_1, \boldsymbol{x}_2)}) \tag{22}$$

instead of its Carnahan–Starling approximation ($4v_0$), namely

$$\Psi(\eta) = \left(\frac{B_2}{v_0} - 4\right)\eta + \eta\frac{(4-3\eta)}{(1-\eta)^2} \tag{23}$$

where $\eta = v_0\bar{\rho}(\boldsymbol{r})$ with v_0 being the volume of a molecule (see [11] for details).

4.2. Discotic molecules

The density functional of equations (18)–(20) can be used for theoretical studies of the phase behaviour of both prolate (rodlike) and oblate (disclike) non-spherical molecules. Such studies always face two non-trivial technical problems. First, the interaction potential between two non-spherical molecules, $V(\boldsymbol{x}_1, \boldsymbol{x}_2) \equiv V(\boldsymbol{r}_1 - \boldsymbol{r}_2, \boldsymbol{u}_1, \boldsymbol{u}_2)$, is a complicated anisotropic object depending, as well as on the distance r_{12}, on the relative orientation of the three vectors $\{\boldsymbol{r}_{12}, \boldsymbol{u}_1, \boldsymbol{u}_2\}$. Very little is known about such potentials. In what follows we will use the Gay–Berne potential [30] as a model potential for such molecules. This corresponds to using a (shifted) Lennard-Jones potential for each relative orientation, with an amplitude and range which continuously change when the relative orientation is changed. Since this Gay–Berne potential can be formulated in analytic form its use in conjunction with equations (18)–(20) is indicated because the second, and main, problem raised by these equations concerns the fact that, e.g., equation (19) involves a tenfold integral. Such high order integrals are unavoidable here, because of the increased number of degrees of freedom of the non-spherical molecules, and this turns the minimization of the total density functional into a formidable numerical task. To make this program realizable we will restrict ourselves here to discotic (or oblate) molecules and parametrize $\rho(\boldsymbol{r}, \boldsymbol{u})$ in terms of a small number of well chosen order parameters.

4.3. Order parameters

Besides the uniform and isotropic phase (I), for which $\rho(\boldsymbol{r}, \boldsymbol{u})$ is independent of both $\boldsymbol{r}$ and $\boldsymbol{u}$, a system of non-spherical molecules can, in principle, exhibit a bewildering variety of partially ordered or liquid crystal phases and also several crystalline phases [28]. In what follows we will restrict ourselves to only two liquid-crystal phases, the nematic phase (N) and the columnar phase (Co). The uni-axial nematic phase is a uniform phase for which $\rho(\boldsymbol{r}, \boldsymbol{u})$ takes on the form $\rho h(\boldsymbol{u}\cdot\boldsymbol{n})$, where ρ is the system's average number density and $h(\boldsymbol{u}\cdot\boldsymbol{n})$ the normalized ($\int \mathrm{d}\boldsymbol{u}\, h(\boldsymbol{u}\cdot\boldsymbol{n}) = 1$) angular distribution of the orientation of the molecule ($\boldsymbol{u}$) relative to the nematic director $\boldsymbol{n}$ ($\boldsymbol{n}^2 = 1$). Such phases are known to exist for both oblate and prolate molecules. To describe them we will use a simple Maier–Saupe order parameter γ by taking $h(\boldsymbol{u}\cdot\boldsymbol{n}) \propto \exp\{\gamma P_2(\boldsymbol{u}\cdot\boldsymbol{n})\}$, where $P_2(x)$ is the second Legendre polynomial describing the quadrupolar order characteristic of the N-phase. The columnar phase plays, for oblate molecules, a role similar to that of the smectic phase for prolate molecules. Several types of Co-phase can be found [31], but here we will restrict ourselves to a phase for which $\rho(\boldsymbol{r}, \boldsymbol{u})$ can be approximated as $\rho h(\boldsymbol{u}\cdot\boldsymbol{n})g(\boldsymbol{R})$, where $\boldsymbol{R}$ are the coordinates in the two directions perpendicular to $\boldsymbol{n}$ and $g(\boldsymbol{R})$ represents a set of Gaussian peaks forming a two-dimensional triangular lattice. In other words, in this Co-phase the nematically ordered ($\gamma \neq 0$) discotic molecules moreover form columns, with the columnar axis parallel to the director $\boldsymbol{n}$, the set of columnar axes forming a triangular lattice, while the molecules are uniformly distributed along these columns. The minimal set of order parameters retained here consists thus of γ and the inverse width of the Gaussians describing the localization of the discotic molecules along the columns.

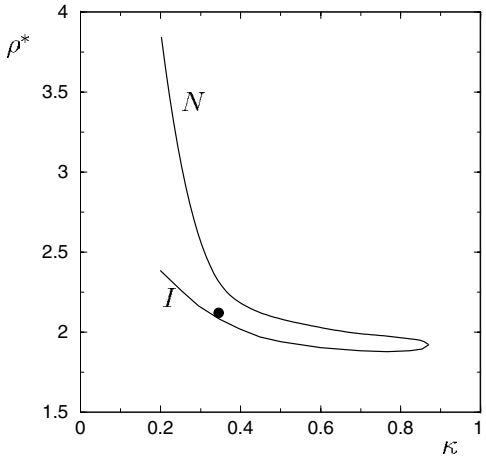

Figure 5. The reduced density, $\rho*$, of the nematic (N) and isotropic (I) phases for an I–N coexistence of discotic molecules of aspect ratio κ for $0.2 < \kappa < 1$. The black dot represents a simulation result [12] for which the density gap ($\rho_N^* - \rho_I^*$) was not resolved. Note that for κ larger than a threshold value (here $\kappa \approx 0.88$) the N-phase becomes metastable.

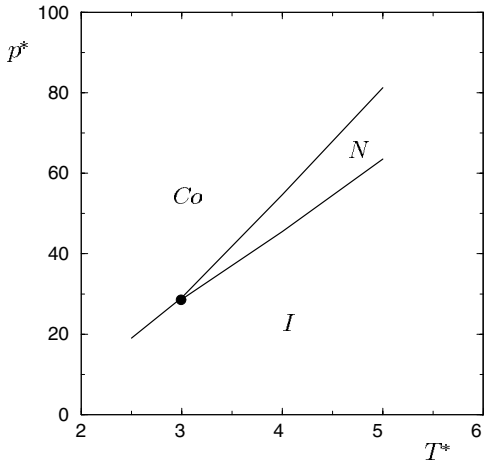

Figure 6. Example of an I–N–Co phase diagram of discotic molecules in the reduced pressure (p^*)-reduced temperature (T^*) plane for $1 < T^* < 5$. Note the I–N–Co triple point (black dot) below which the N-phase becomes metastable.

4.4. Phase transitions

To illustrate the results obtained from equations (18)–(20) we first consider the I–N transition in the absence of the Co-phase. As is well known, the anisotropic N-phase can exist only for non-spherical molecules. If we characterize the aspect ratio of a uni-axial centro-symmetric molecule by κ ($0 < \kappa < 1$ for oblate molecules) it is seen from figure 5 that the I–N transition is always first order with a density gap, $\Delta\rho = \rho_N - \rho_I$, which decreases when κ increases (i.e. when the molecules become more spherical) until a maximum value of κ is attained above which the N-phase is no longer stable. Next, when the Co-phase is allowed to compete with the I- and N-phases it is found (see figure 6) that the resulting phase diagram exhibits an I–N–Co triple point, below which the N-phase is metastable and only the I–Co transition remains, whereas above this triple point the I–N transition is followed by a N–Co transition. This theoretical scenario is in qualitative (but not quantitative) agreement with recent simulation results [12].

5. Conclusions

We have shown that DFT is an adequate and flexible tool to describe the phase behaviour of simple models of soft matter systems. We have considered both polydisperse systems of spherical colloidal particles and monodisperse systems of non-spherical, disclike, particles. On the basis of a simple vdW-like model we have studied the fractionation of an initial polydisperse bulk fluid phase into two polydisperse fractions, one fluid and the other either fluid or solid. The non-trivial segregation of the small particles in a spatially non-uniform polydisperse fluid has been illustrated for the case of a fluid–fluid interface and for a fluid in a external gravity field. Finally, it has been shown that a simple DFT can describe the phase behaviour of monodisperse systems of disc-shaped particles in qualitative agreement with computer simulations.

Acknowledgment

MB acknowledges financial support from the FNRS.

References

[1] Evans R 1979 *Adv. Phys.* **28** 143
[2] see e.g.,
Henderson D 1992 *Fundamentals of Inhomogeneous Fluids* (New York: Dekker)
Lowen H 1994 *Phys. Rep.* **237** 249
[3] See, e.g.,
Lutsko J and Baus M 1990 *Phys. Rev. Lett.* **64** 761
Denton A R and Ashcroft N W 1989 *Phys. Rev.* A **39** 4701
[4] Xu H and Baus M 1992 *J. Phys.: Condens. Matter* **4** L663
[5] Pusey P 1991 *Liquids, Freezing and Glass Transition* ed J P Hansen, D Levesque and J Zinn-Justin (Amsterdam: North-Holland) p 763
[6] Bellier-Castella L, Xu H and Baus M 2000 *J. Chem. Phys.* **113** 8337
[7] Bellier-Castella L, Baus M and Xu H 2001 *J. Chem. Phys.* **115** 3381
[8] Xu H and Baus M, in preparation
[9] Bellier-Castella L, Xu H and Baus M 2002 *Phys. Rev.* E **65** 021503-1
[10] Bellier-Castella L and Xu H, in preparation
[11] Coussaert T and Baus M 2002 *J. Chem. Phys.* **116** 7744
[12] Bellier-Castella L, Caprion D and Ryckaert J P, in preparation
[13] See, e.g.,
van Megen W, Mortensen T C and Williams S R 1998 *Phys. Rev.* E **58** 6073
[14] van der Kooij F M, Kassapidou K and Lekkerkerker H N W 2000 *Nature* **406** 868
[15] See, e.g.,
de Hoog E H A and Lekkerkerker H N W 1999 *J. Phys. Chem.* B **103** 5274
Brader J M and Evans R 2000 *Europhys. Lett.* **49** 678
[16] Salacuse J J and Stell G 1982 *J. Chem. Phys.* **77** 3714
[17] See, e.g.,
Gualtieri J A, Kincaid J M and Morrison G 1982 *J. Chem. Phys.* **77** 521
Briano J B and Glandt E D 1984 *J. Chem. Phys.* **80** 3336
[18] Sollich P and Cates M E 1998 *Phys. Rev. Lett.* **80** 1365
Warren P B 1998 *Phys. Rev. Lett.* **80** 1369
Sollich P 2002 *J. Phys.: Condens. Matter* **14** R79
[19] Evans R M L, Fairhurst D J and Poon W C K 1998 *Phys. Rev. Lett.* **81** 1326
[20] Xu H and Baus M 2000 *Phys. Rev.* E **61** 3249
[21] Bartlett P and Warren P B 1999 *Phys. Rev. Lett.* **82** 1979
[22] Barrat J L and Hansen J P 1986 *J. Physique* **47** 1547
[23] Bolhuis P and Kofke D A 1996 *Phys. Rev.* E **54** 634
[24] Daanoun A, Tejero C F and Baus M 1994 *Phys. Rev.* E **50** 2913
[25] Hansen J P and McDonald I R 1986 *Theory of Simple Liquids* 2nd edn (London: Academic)
[26] Biben T and Hansen J P 1994 *J. Phys.: Condens. Matter* **6** A345
[27] Pagonabarraga I, Cates M E and Ackland G G 2000 *Phys. Rev. Lett.* **84** 911
[28] Onsager L 1949 *Ann. NY Acad. Sci.* **51** 627
[29] Ponienierski A and Holyst R 1988 *Phys. Rev. Lett.* **61** 2461
[30] Gay J G and Berne B 1981 *J. Chem. Phys.* **74** 3316
[31] Oswald P and Pieranski P 2000 *Les Cristaux Liquides* (Paris: Gordon and Breach)